Journal of Peptide Science
J. Peptide Sci. **11**: 365–378 (2005)
Published online 10 January 2005 in Wiley InterScience (www.interscience.wiley.com). DOI: 10.1002/psc.637

JOURNAL OF PEPTIDE SCIENCE

Examination of structural characteristics of the potent oxytocin antagonists (dPen^1,Pen^6)-OT and (dPen^1,Pen^6, 5-*t*BuPro^7)-OT by NMR, raman, CD spectroscopy and molecular modeling‡

LAURENT BÉLEC, JOHN W. BLANKENSHIP and WILLIAM D. LUBELL*

Département de Chimie, Université de Montréal, C. P. 6128, Succursale Centre Ville, Montréal, Québec, H3C 3J7, Canada

Received 4 October 2002; *Revised 4 October 2004*; *Accepted 5 October 2004*

Abstract: The synthesis and biological evaluation of penicillamine^6-5-*tert*-butylproline^7-oxytocin analogs and comparison with their proline^7-oxytocin counterparts has led to the discovery of two potent oxytocin (OT) antagonists: [dPen^1,Pen^6]-oxytocin (**1**, $pA_2 = 8.22$, $EC_{50} = 6.0$ nM) and [dPen^1,Pen^6,5-*t*BuPro^7]-oxytocin (**2**, $pA_2 = 8.19$, $EC_{50} = 6.5$ nM). In an attempt to understand the conformational requirements for their biological activity, spectroscopic analyses of **1** and **2** were performed using ^{1}H NMR, laser Raman and CD techniques. In H_2O, oxytocin analogs **1** and **2** exhibited *cis*-isomer populations of 7% and 35%, respectively. Measurement of the amide proton temperature coefficients revealed solvent shielded hydrogens for Gln^4 and Pen^6 in the major *trans*-conformer of **1** as well as for Gln^4 in the minor *cis*-conformer of **2**. Few long-distance NOEs were observed, suggesting conformational averaging for analogs **1** and **2** in water; moreover, a lower barrier (16.6 ± 0.2 kcal/mol) for isomerization of the amide *N*-terminal to 5-*t*BuPro^7 relative to OT was calculated from measuring the coalescence temperature of the Gly^9 backbone NH signals in the NMR spectra of **2**. Observed bands in the Raman spectra of **1** and **2** correspond to C_β-S-S-C_β dihedral angles of $+110$–115° and $\pm 90^\circ$, respectively. In water, acetonitrile and methanol, the CD spectra for **1** exhibited a positive maximum around 236–239 nm; in trifluoroethanol, the spectra shifted and a negative maximum was observed at 240 nm. The CD spectra of **2** were unaffected by solvent changes and exhibited a negative maximum at 236–239 nm. The CD and Raman data both suggested that a conformation having a right-handed screw sense about the disulfide and a χ_{CS-SC} dihedral angle value close to 115° was favored for analog **1** in water, methanol and acetonitrile, but not trifluoroethanol, where a $\pm 90^\circ$ angle was favored. Analog **2** was more resilient to conformational change about the disulfide, and adopted a preferred disulfide geometry corresponding to a $\pm 90^\circ$ χ_{CS-SC} dihedral angle. Monte Carlo conformational analysis of analogs **1** and **2** using distance restraints derived from NMR spectroscopy revealed two prominent conformational minima for analog **1** with disulfide geometries around $+114^\circ$ and $+116^\circ$. Similar analysis of analog **2** revealed one conformational minimum with a disulfide geometry around $+104^\circ$. In sum, the conformation about the disulfide in [dPen^1,Pen^6]-OT (**1**) was shown to be contingent on environment and in TFE, adopted a geometry similar to that of [dPen^1,Pen^6,5-*t*BuPro^7]-OT (**2**) which appeared to be stabilized by hydrophobic interactions between the 5-*t*BuPro^7 (5*R*)-*tert*-butyl group, the Leu^8 isopropyl sidechain and the Pen^6 β-methyl substituents. In light of the conformational rigidity of **2** about the disulfide bond, and the similar geometry adopted by **1** in TFE, a S-S dihedral angle close to $+110^\circ$ may be a prerequisite for their binding at the receptor.

Keywords: oxytocin; peptide conformation; proline; 5-*tert*-butylproline; amide isomers; disulfide geometry

INTRODUCTION

Conformationally rigid analogs of biologically active peptides are important for studying G-protein coupled receptor (GPCR) interactions that operate in signal transduction [1]. In structure–activity relationship (SAR) investigations, they can help elucidate the three-dimensional structure responsible for biological activity. For example, attempts to define the conformational prerequisites for the activity of the peptide hormone oxytocin (OT) **3** at its receptor have led to the synthesis of various analogs incorporating modifications to the peptide backbone, amino acid sequence, ring size and side-chain functional groups [2–6].

Mainly responsible for lactation and uterine contractions in mammals, OT has been used clinically to induce rhythmic contractions of the uterus in pregnant women since the 1950s [7–9]. Inhibitors of oxytocin activity have been clinically evaluated over the past 20 years as treatments of preterm labor [4,10–13]. For example, Atosiban [Mpa^1,D-Tyr(OEt)^2,Thr^4,Orn^8-OT] **4** is used clinically in Europe to treat preterm labor [14]. A more detailed understanding of the conformational requirements for biological activity of OT analogs is thus essential for the rational design of drugs that regulate activity at its receptor.

In the 1970s, conformational analyses of several OT analogs led to the proposal of two models describing

* Correspondence to: Professor William D. Lubell, Département de Chimie, Université de Montréal, C.P. 6128, Succursale Centre Ville, Montréal, Québec, H3C 3J7, Canada;
e-mail: lubell@chimie.umontreal.ca
‡ Dedicated to the memory of professor Murray Goodman, deceased 1 June 2004.

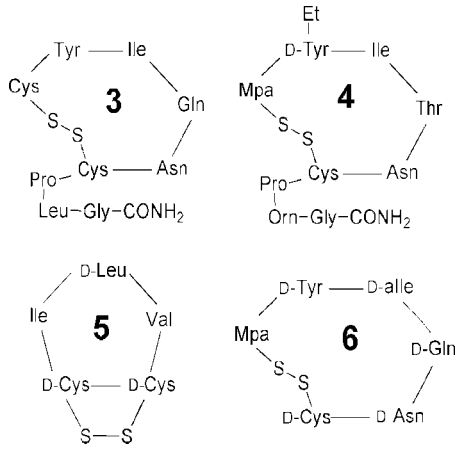

Figure 1 Structures of oxytocin **3**, atosiban **4**, malformin A_1 **5** [69]and retro-D-tocinamide **6** [65].

the structural requirements for biological activity: the cooperative model and the dynamic model [15–18]. In the cooperative model, two β-turns, centered on Ile^3-Gln^4 and Pro^7-Leu^8, create a sheet-like structure with hydrophilic and hydrophobic residues on opposite sides. According to this model the side-chains of Tyr^2 and Asn^5 interact in a way responsible for signal transduction. The dynamic model refers to the conformational flexibility of oxytocin analogs [17,18]. Based on biophysical studies, it concludes that the macrocyclic portion and certain side chains of antagonist analogs are less flexible. In particular, the Ile^3 and Asn^5 amide hydrogens are shielded from solvent inside the cyclic portion of the peptide such that the lipophilic and hydrophilic residues are on opposite sides of the peptide. The prerequisites for biological activity of OT analogs that were predicted by these models still hold true today after the synthesis of hundreds of analogs featuring systematic modifications that have refined the conformation and location of turns within the macrocycle, altered the chirality and structure of side chains such as those of Tyr^2 and Asn^5, and modified the amides involved in hydrogen bonding [5].

Two structural features of OT analogs that have been more recently associated with biological activity are the geometry of the disulfide bond and the amide *N*-terminal to proline[7]. Since the x-ray crystal structure of Mpa^1-OT revealed two conformers in the crystal unit that differed mainly in their disulfide bond geometry (one exhibiting right-handed *P*-helicity (+76°)[§] and the other left-handed *M*-helicity (−101°), Figure 2 and 3) [19,20], the handedness of the disulfide has been suggested as a determinant for activity: right-handed *P*-helicity has been suggested to be adopted by antagonists, and left-handed *M*-helicity to be adopted by agonists [19]. Although both conformers in the crystal structure of Mpa^1-OT possessed the amide *N*-terminal to proline[7] in the *trans*-isomer conformation, an NMR spectroscopic study of OT (**3**) demonstrated that the amide *N*-terminal to Pro^7 could adopt up to 10% *cis*-isomer in solution [21,22]. Furthermore, conformational analyses of the potent bicyclic OT antagonists [Mpa^1,*cyclo*(Glu^4,Lys^8)]-OT and [$dPen^1$,*cyclo*(Glu^4,Lys^8)]-OT by NMR spectroscopy (DMSO) and molecular modeling revealed the disulfide bond to be flexible and the prolyl amide locked in the *cis*-isomer conformation [23]. Comparison of these bicyclic analogs and other OT analogs has led to the hypothesis that the prolyl amide *trans*-isomer is necessary for agonist activity and that the *cis*-isomer may favor antagonism [24].

To improve the understanding of the relationship between the structure and biological activity of OT antagonists, the steric interactions of alkyl group substituents were used to modify peptide conformation. Recently, the synthesis and biological evaluation was reported of six penicillamine[6]-oxytocin analogs, five of which had not previously been reported [25]. Two analogs exhibited strong inhibition of OT activity: [$dPen^1$,Pen^6]-OT (**1**) and [$dPen^1$,Pen^6,5-*t*BuPro^7]-OT (**2**). Although the amide *N*-terminal to 5-*tert*-butylproline in the latter analog exhibited a 5-fold greater *cis*-isomer population (35% for **2** and 7% for **1**) relative to its proline counterpart, the *trans*-amide conformer still predominated. Furthermore, their conformational differences, observed in water, did not have a significant

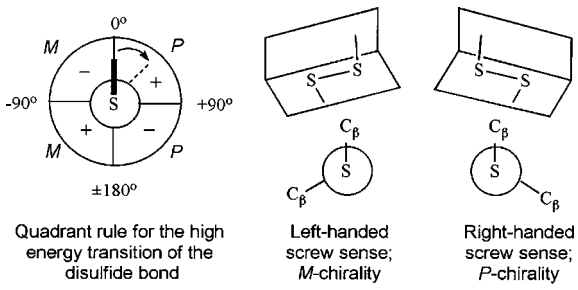

Figure 2 Illustrations of disulfide helicity and quadrant rule.

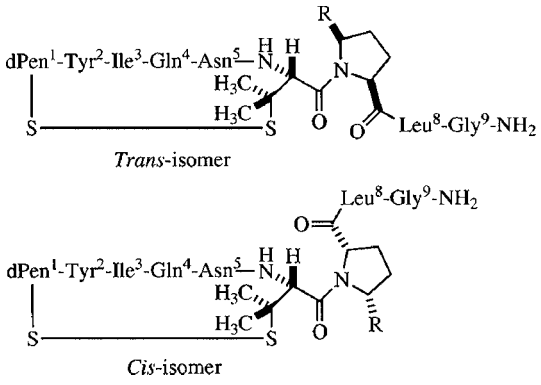

Figure 3 Prolyl amide isomers of [$dPen^1$,Pen^6]-OT (**1**, R = H) and [$dPen^1$,Pen^6,5-*t*BuPro^7]-OT (**2**, R = *t*-Bu).

§ For rules of nomenclature concerning helicity see reference [88].

impact on their uterotonic potency ($pA_2 = 8.22$, $EC_{50} = 6.0$ nM for **1** and $pA_2 = 8.19$, $EC_{50} = 6.5$ nM for **2**) nor receptor affinity ($K_i = 37$ nM for **1** and 33 nM for **2**) as measured *in vitro* on the rat uterine receptor [25]. The apparent discrepancy between conformation and biology of peptides **1** and **2** warranted further investigation to better understand the significance of conformation for antagonist activity of these OT analogs. This paper reports the conformational study of these oxytocin antagonists using NMR, Raman and CD spectroscopy in conjunction with molecular modeling.

MATERIALS AND METHODS

Synthesis and Biological Evaluation of Peptides

The synthesis and biological evaluation of peptide analogs **1** and **2** has been described previously [25].

NMR Measurements

^{1}H NMR experiments were performed on a Bruker DMX600 spectrometer. The chemical shifts are reported in ppm (δ units). Coupling constants are in Hz. For temperature coefficient ($\Delta\delta/\Delta T$) determinations, six ^{1}H NMR spectra were recorded at 5° intervals from 303 to 328 K, with dioxane as an internal standard. COSY, TOCSY and ROESY spectra were obtained on 3.0 mM samples in 9 : 1 H_2O : D_2O and 3.5 mM samples in D_2O at pH 6.5 without added buffer. Some ^{1}H NMR, NOESY and ROESY spectra were also recorded at pH ≈ 3.5 by adding CD_3CO_2D. Spectra were measured at 303 K with 2048 by either 512 or 1024 data points with mixing times of 70 and 107 ms for the TOCSY spectra; 100, 200, 300 and 500 ms for the NOESY spectra; 100, 200, 250 and 500 ms for the ROESY spectra. At 288 K in D_2O, additional ROESY spectra were obtained with 2048 by either 320 or 400 data points and a 250 ms mixing time. Distance restraints were generated from intermolecular NOEs observed in the ROESY spectra with a 250 ms mixing time using the intensity-ratio method [26]; peak volumes were corrected for the ROESY offset dependence [27], and the intraresidue NOE between the meta and ortho ring hydrogens of Tyr was used as a reference distance (2.47 Å). Peak volumes from at least three experiments were used to generate each distance restraint.

Laser Raman Spectroscopy

Raman spectra were obtained with a Renishaw imaging microscope using a 782.0 nm diode laser (near infrared) excitation, with 5 mW of power at the sample. A 50× objective was used to focus the laser on a 2 μm area. Spectral acquisition was effected with a coupled charge detector (CCD; 15 × 576) and a resolution of 2 cm^{-1}. Spectra were recorded on solid lyophilized samples between 1800 cm^{-1} and 400 cm^{-1} with acquisition times of 300 s per scan for ten scans, which were averaged to obtain each spectrum. Due to the great sensitivity of the CCD detector, a cosmic ray filter was employed.

Circular Dichroism

The CD spectra were obtained on a Jasco J-710 spectropolarimeter, using a 1 cm cell length and a concentration of 0.1 mg/ml of peptides **1** and **2** (for each solvent) at 25 °C. The CD spectra were recorded with a sensitivity of 100 mdeg, a resolution of 0.2 nm, a bandwidth of 1.0 nm, a response time of 0.25 s, and a scan speed of 100 nm/min. Five scans were averaged for each spectrum. Units for [θ] values are deg × cm^2 × $decimole^{-1}$.

Molecular Modeling

Molecular modeling was carried out using Macromodel 8.5 [28] (Schrödinger, Portland, OR) on a Pentium 4 personal computer running Red Hat Linux 9. All minimization and conformational searches were done within a GB/SA continuum model with extended electrostatics and force field charges to mimic aqueous solvation [29,30]; initial calculations were carried out using the AMBER* force field implementation [31–33] in Macromodel, and later repeated using the OPLS-AA force field [34,35] for the final calculations, owing to the higher quality disulfide parameters in OPLS-AA [35]. The Polak-Ribière Conjugate Gradient method [36] was used in all minimization steps. Models of analogs **1** and **2** were built within Macromodel and minimized. Initial Monte Carlo conformational searches [37,38] were carried out in the absence of restraints. Subsequent Monte Carlo conformational searches [37,39] on **1** and **2** used 16 and 9 inter-residue distance constraints, respectively. In the final round of searching on **2**, a C_β-S-S-C_β angle restraint of 90° ± 5° was introduced as well. For each conformational search experiment, 5000–10 000 structures were generated, and 2000 minimization steps were used. Convergence was assessed within and between experiments; the conformational search was halted when no additional low energy conformations were found. This process completed after 35 000 structures were generated for analog **1** and 80 000 structures were generated for analog **2**. Rebuilding the structures with the opposite disulfide geometry (*M* helicity) and repeating the conformational search resulted in convergence at structures with *P* helicity. Electrostatic calculations were carried out using APBS [40] with the non-linear Poisson-Boltzmann equation [41,42] and visualized in PyMOL [43].

RESULTS AND DISCUSSION

Conformational Analysis by NMR Spectroscopy

As previously reported, both analogs **1** and **2** were observed to exhibit prolyl amide equilibrium by ^{1}H NMR spectroscopy [25]. Proton resonance chemical shifts were determined for residues of major and minor conformations of peptides **1** and **2** using COSY, TOCSY and ROESY ^{1}H NMR experiments (Table 1) [26]. The major and minor sets of signals observed in the spectra of **1** and **2** were attributed to the *trans*- and *cis*-isomers *N*-terminal to the proline[7] and 5-*tert*-butylproline[7], respectively, based on NOE cross-peaks observed between their α- and δ-protons with the α-proton of penicillamine[6] [25]. Certain residues (dPen[1], Ile[3], Gln[4], Asn[5], Pen[6] and Pro[7]) of the less populated proline[7] amide *cis*-isomer conformer of peptide **1** were not detected and thus not assigned. The NH-C_αH coupling constants were measured, ϕ dihedral angles

were calculated, and $C_\alpha H_i$-NH_{i+1} NOEs were used to confirm the sequential connectivities (Tables 2–4) [26,44,45]. Other than the expected $C_\alpha H_i$-NH_{i+1} and some NH_i-NH_{i+1}, only a few inter-residue NOEs were detected (Table 4) [26,46], despite the recording of multiple ROESY and NOESY spectra for both analogs with mixing times ranging from 100 to 500 ms using different pulse sequences. Although the maximum intensity of the NOE signals was observed at 250 and 300 ms, application of these optimum mixing times and recording of the ROESY spectra at 278 K together gave no additional observable NOE signals. This result combined with the observation that most (6/7) of the $J_{NH-C\alpha H}$ values were in the conformational averaging range (5–8 Hz), suggested that peptides **1** and **2** were flexible and adopted multiple conformations in water. Nonetheless, the weak Tyr^2 NH and Asn^5 NH NOE observed in the spectra for the major conformer of analog **1** suggested less than a 5 Å separation of these residues, indicative of a turn bordered by the Tyr^2 and

Table 1 ^{1}H NMR Data for [dPen^1,Pen^6]-OT (**1**) and [dPen^1,Pen^6,5-*t*BuPro^7]-OT (**2**) in Water

Residue	**1**		**2**		Residue	**1**		**2**	
	Major	Minor	Major	Minor		Major	Minor	Major	Minor
dPen^1					Asn^5				
$C_\alpha H$	2.48	—	2.51	2.56	NH	8.31	—	8.22	8.29
$C_\alpha H$	2.31	—	2.34	2.29	$C_\alpha H$	4.72	—	4.64	4.60
$C_\gamma H_3$	1.29	—	1.25	1.25	$C_\beta H$	2.77	—	2.77	2.80
$C_\gamma H_3$	1.29	—	1.18	1.22	$C_\beta H$	2.68	—	2.77	2.71
Tyr^2					$J_{\alpha\beta D}$	5.5	—	7.7	5.0
NH	8.23	8.21	8.15	8.22	$J_{\alpha\beta U}$	—	—	7.9	9.5
$C_\alpha H$	4.52	4.53	4.50	4.57	$J_{\beta\beta}$	—	—	—	16.4
$C_\beta H$	3.11	3.12	3.12	3.12	J_{NHCH}	8.16	—	7.6	7.3
$C_\beta H$	2.94	2.88	2.94	2.90	Pen^6				
$C_m H$	7.11	(7.11)	7.11	7.12	NH	7.70	—	8.07	7.61
$C_o H$	6.80	(6.80)	6.80	6.79	$C_\alpha H$	4.55	—	5.17	4.58
$J_{\alpha\beta}$	—	—	6.2	6.2	$C_\gamma CH_3$	1.34	—	1.39	(1.26)
$J_{\alpha\beta}$	—	—	7.7	8.3	$C_\gamma CH_3$	1.33	—	1.26	(1.22)
$J_{\delta\varepsilon}$	8.6	(4.8)	8.5	8.5	J_{NHCH}	6.6	—	—	7.8
J_{NHCH}	7.1	7.7	7.4	(7.0)	Pro^7 or 5-*t*-BuPro^7				
Ile^3					$C_\alpha H$	4.36	—	4.57	4.78
NH	7.73	—	7.93	7.75	$C_\beta H$	2.21	—	2.19	2.32
$C_\alpha H$	4.13	—	4.08	4.12	$C_\beta H$	2.01	—	2.07	2.09
$C_\beta H$	1.91	—	1.91	1.89	$C_\gamma H$	1.93	—	2.00	1.91
$C_\gamma CH_2$	1.22	—	1.30	1.29	$C_\gamma H$	1.85	—	1.75	1.83
$C_\gamma CH_3$	1.01	—	1.06	1.07	$C_\delta H$	3.83	—	3.81	4.09
$C_\delta CH_3$	0.81	—	0.85	0.86	$C_\delta H$	3.65	—	—	—
$J_{\alpha\beta}$	(6.1)	—	7.0	(7.1)	*t*-Bu	—	—	0.91	0.81
J_{NHCH}	6.9	—	7.0	6.4	Leu^8				
Gln^4					NH	8.37	8.43	7.94	8.35
NH	7.78	—	7.73	7.69	$C_\alpha H$	4.24	4.15	4.24	4.17
$C_\alpha H$	4.10	—	4.22	4.16	$C_\beta H$	1.63	1.59	1.59	1.61
$C_\beta H$	2.06	—	2.06	2.03	$C_\beta H$	1.53	—	1.55	1.55
$C_\beta H$	2.00	—	1.96	1.97	$C_\delta H_3$	0.87	0.88	0.84	0.88
$C_\gamma H$	2.29	—	2.29	2.29	$C_\delta H_3$	0.82	0.83	—	—
$C_\gamma H$	2.29	—	2.29	2.29	$J_{\alpha\beta}$	(5.0)	—	6.8	—
$J_{\alpha\beta}$	8.8	—	(6.0)	(6.4)	$J_{\gamma\delta}$	6.5	—	—	—
J_{NHCH}	5.8	—	7.0	(6.7)	J_{NHCH}	6.8	5.1	6.5	7.2
					Gly^9				
					NH	8.32	8.48	8.45	8.46
					$C_\alpha H$	3.84	3.86	3.87	3.87
					$C_\alpha H$	3.84	3.79	3.77	3.77
					$J_{\alpha\alpha}$	15.5	16.1	17.2	17.2
					J_{NHCH}	6.1	5.7	6.3	5.4

— not observed; () overlap.

Table 2 Coupling Constant ($^3J_{NH-H\alpha}$) and ϕ Dihedral Angle Correlations for **1**

Residue	Major			Minor		
	$^3J_{NH-H\alpha}$[a] (θ^1) [θ^2][b]	ϕ[b]	ϕ[c]	$^3J_{NH-H\alpha}$[a] (θ^1) [θ^2][b]	ϕ[b]	ϕ[c]
Tyr^2	7.1	40.5		7.7	48.9	
	(19.5)	79.5		(11.1)	71.1	
	[145.7]	−85.7	−83.0	[149.9]	−89.9	−88.1
		−154.3	−157.0		−150.1	−151.9
Ile^3	6.9	38.4	38.4	—		
	(21.6)	81.6	60.0			
	[144.4]	−84.4	−81.4			
		−155.6	−158.6			
Gln^4	5.8	28.5	33.8	—		
	(31.5)	91.5	86.2			
	[137.4]	−77.4	−72.8			
		−162.6	−167.2			
Asn^5	8.2	−93.6	−92.7	—		
	[153.6]	−146.4	−147.3			
Pen^6	6.6	35.4	46.7	—		
	(24.6)	84.6	73.3			
	[142.5]	−82.5	−79.0			
		−157.5	−161.0			
Leu^8	6.8	37.3	52.4	5.1	23.1	25.6
	(22.7)	82.7	67.6	(36.9)	96.9	94.4
	[143.8]	−83.8	−80.6	[133.1]	−73.1	−67.3
		−156.2	−159.4		−166.9	−172.7
Gly^9	6.1	31.0	37.9	5.7	27.7	32.6
	(29.0)	89.0	82.1	(32.3)	92.3	87.4
	[139.3]	−79.3	−75.1	[136.8]	−76.8	−72.0
		−160.7	−164.9		−163.2	−168.0

[a] In Hz (±0.3), determined at 30 °C and pH ≈ 6.5 in 9 : 1 $H_2O : D_2O$. — , not observed.
[b] Calculated according to Bystrov [45]: $^3J_{NH-H\alpha} = 8.6\cos^2\theta - 1.0\cos\theta + 0.4$, where $\theta = |\phi - 60|$; $\pm\theta^1$ and θ^2 are possible solutions.
[c] Calculated according to Wüthrich [26]: $^3J_{NH-H\alpha} = 6.4\cos^2\theta - 1.4\cos\theta + 1.9$, where $\theta = |\phi - 60|$.
Values are reported following IUPAC-IUB nomenclature.
‡ For examples and illustrations of θ to ϕ correlations see references [24], [26] (and references 26 and 27 therein), and [45].

Table 3 Coupling Constant ($^3J_{NH-H\alpha}$) and ϕ Dihedral Angle Correlations for **2**

Residue	Major			Minor		
	$^3J_{NH-H\alpha}$[a] (θ^1) [θ^2][b]	ϕ[b]	ϕ[c]	$^3J_{NH-H\alpha}$[a] (θ^1) [θ^2][b]	ϕ[b]	ϕ[c]
Tyr^2	7.4	44.2		—		
	(15.8)	75.8				
	[147.7]	−87.8	−85.5			
		−152.3	−154.5			
Ile^3	7.0	39.4		6.4	33.6	42.7
	(20.6)	80.6		(26.4)	86.4	77.3
	[145.1]	−85.1	−82.2	[141.2]	−81.2	−77.4
		−154.9	−157.8		−158.8	−162.6
Gln^4	7.0	39.4		6.7	36.3	49.2
	(20.6)	80.6		(23.7)	83.7	70.8
	[145.1]	−85.1	−82.2	[143.1]	−83.1	−79.8
		−154.9	−157.8		−156.9	−160.2
Asn^5	7.6	47.2		7.3	42.9	
	(12.8)	72.8		(17.1)	77.1	
	[149.2]	−89.2	−87.2	[147.1]	−87.1	−84.7
		−150.8	−152.8		−152.9	−155.3
Pen^6	—			7.8	51.0	
				(9.0)	69.0	
				[150.6]	−90.6	−89.0
					−149.4	−151.0
Leu^8	6.5	34.5	44.6	7.2	41.7	
	(25.5)	85.5	75.4	(18.3)	78.3	
	[141.8]	−81.8	−78.2	[146.4]	−86.4	−83.8
		−158.2	−161.8		−153.6	−156.2
Gly^9	6.3	32.7	41.0	5.4	25.4	29.0
	(27.3)	87.3	79.0	(34.6)	94.6	91.0
	[140.5]	−80.5	−76.6	[135.0]	−75.0	−69.7
		−159.5	−163.4		−165.0	−170.3

[a] In Hz (±0.3), determined at 30 °C and pH ≈ 6.5 in 9 : 1 $H_2O : D_2O$. — , not observed.
[b] Calculated according to Bystrov [45]: $^3J_{NH-H\alpha} = 8.6\cos^2\theta - 1.0\cos\theta + 0.4$, where $\theta = |\phi - 60|$; $\pm\theta^1$ and θ^2 are possible solutions.
[c] Calculated according to Wüthrich [26]: $^3J_{NH-H\alpha} = 6.4\cos^2\theta - 1.4\cos\theta + 1.9$, were $\theta = |\phi - 60|$.
Values are reported following IUPAC-IUB nomenclature.
‡ For examples and illustrations of θ to ϕ correlations see references [24], [26] (and references 26 and 27 therein), and [45].

Asn^5 residues. In addition, for the major conformer of **1**, strong NOEs were observed between the $C_\alpha H$ of Asn^5 and the NH of Pen^6, between the $C_\alpha H$ of Pen^6 and the $C_\delta H$ of Pro^7, and between the $C_\alpha H$ of Pro^7 and the NH of Leu^8; a weak NOE was observed between the $C_\beta H$ of Gln^4 and the backbone NH of Asn^5. Strong NOEs were observed between the $C_\alpha H$ of Pen^6 and both the $C_\delta H$ and C_δ *t*Bu of 5-*t*BuPro^7 for the major conformer of **2**. Other than a weak NOE between the $C_\beta H$ of Asn^5 and the NH of Pen^6, no other long-range NOE was observed in the spectra for the major conformer of **2** and few NH_i-NH_{i+1} NOEs were detected. These spectral variations indicated conformational differences for **1** and **2** in water; moreover, the lack of long distance NOEs signified considerable conformational averaging of both peptides on the NMR time-scale.

In model peptides, (2*S*,5*R*)-5-*tert*-butylproline (5-*t*BuPro) was shown to possess a lower barrier of isomerization about its *N*-terminal amide bond relative to proline (16.5 vs 20.4 kcal/mol, respectively, for their *N*-acetyl *N*′-methylamide derivatives in water) [47]. By measuring the coalescence temperature (313 K) for the major and minor NH signals of Gly^9 in the 5-*t*BuPro analogue **2**, the $\Delta G^‡$ was approximated to be 16.6 ± 0.2 kcal/mol. This value was significantly

Table 4 Inter-residue NOEs for **1** and **2**

NOE				**1**[a]	**2**
dPen[1]	$C_\alpha H$	Tyr[2]	NH	m	m
dPen[1]	$C_\alpha H'$	Tyr[2]	NH	w	m
Tyr[2]	$C_\alpha H$	Ile[3]	NH	m	w
Tyr[2]	NH	Asn[5]	NH	w	—
Tyr[2]	NH	Asn[5]	$C_\alpha H$	[m]	—
Ile[3]	$C_\alpha H$	Gln[4]	NH	m	m(w)
Ile[3]	NH	Tyr[2]	NH	m	—
Gln[4]	$C_\alpha H$	Asn[5]	NH	m	w(w)
Gln[4]	$C_\beta H$	Asn[5]	NH	w	—
Asn[5]	$C_\alpha H$	Pen[6]	NH	s	w
Asn[5]	NH	Gln[4]	NH	m	—
Asn[5]	NH	Pen[6]	NH	m	—
Asn[5]	$C_\beta H$	Pen[6]	NH	—	w
Pen[6]	$C_\alpha H$	Pro[7]	$C_\delta H$	s	
Pen[6]	$C_\alpha H$	Pro[7]	$C_\delta H'$	m	
Pen[6]	$C_\gamma CH_3$	Pro[7]	$C_\delta H$	m	
Pen[6]	$C_\gamma CH_3$	Pro[7]	$C_\delta H'$	w	
Pen[6]	$C_\alpha H$	*t*BuPro[7]	$C_\delta H$		s
Pen[6]	$C_\alpha H$	*t*BuPro[7]	C_δ *t*Bu	s	
Pro[7]	$C_\alpha H$	Leu[8]	NH	s	
*t*BuPro[7]	$C_\alpha H$	Leu[8]	NH		m(w)
Leu[8]	$C_\alpha H$	Gly[9]	NH	m	m(w)
Leu[8]	NH	Gly[9]	NH	m	—

[a] Values in square brackets represent possible artifacts. Values in parentheses are for the minor *cis* isomer.
— , not observed. w, weak; m, medium; s, strong.

lower than $\Delta G^{\ddagger}$ values calculated for isomerization *N*-terminal to Pro[7] in OT and arginine vasopressin (20.8 and 20.6 kcal/mol, respectively) [22]. Isomerization about the amide *N*-terminal to 5-*t*BuPro[7] may thus account in part for the conformational averaging observed with peptide **2**.

Temperature coefficients were calculated for backbone amide hydrogens of peptides **1** and **2** in water after recording ^{1}H NMR spectra at 5 K intervals between 303 K and 328 K (Table 5). In the major prolyl amide *trans*-isomer of **1**, the backbone amide hydrogens of Gln[4] and Pen[6] exhibited temperature coefficients indicative of solvent shielding ($\Delta\delta/\Delta T > -3 \times 10^{-3}$ ppm/K) [21,48] and hydrogen bonding, suggesting possible turns around these residues. In the major prolyl amide *trans*-isomer of **2**, the temperature coefficients of the same amide hydrogens (Gln[4] and Pen[6]) were in the intermediate range between solvent shielded and solvent exposed hydrogens ($-3 > \Delta\delta/\Delta T > -6 \times 10^{-3}$ ppm/K) indicating the absence of strong hydrogen bonding. In the minor prolyl amide *cis*-isomer conformation of **2**, a temperature coefficient was measured for the backbone amide of Gln[4] that was consistent with solvent shielding, and intermediate range temperature coefficient values were observed for Ile[3], Pen[6] and Leu[8]. Due to its small population, most of the hydrogen amide resonances for the minor *cis*-isomer conformation of **1** were not detected. Temperature coefficients consistent with solvent shielded hydrogens were previously observed in the studies of antagonist analog [Pen[1]]-OT ($pA_2 = 6.9$) for Ile[3] and Asn[5] [17]; and in the bicyclic antagonists [Mpa[1],*cyclo*(Glu[4],Lys[8])]-OT ($pA_2 = 8.2$) and [dPen[1],*cyclo*(Glu[4],Lys[8])]-OT ($pA_2 = 8.7$) for Ile[3] and Glu[4] [23]. Temperature coefficients were also calculated for the NH_2 amide proton resonances of Gln[4], Asn[5] and Gly[9] in analogs **1** and **2** (data not shown) and the $\Delta\delta/\Delta T$ values ranged from −6.5 to -4.3×10^{-3} ppm/K indicating the absence of strong hydrogen bonding.

Table 5 Temperature Coefficients ($\Delta\delta/\Delta T$) for Amide Proton Resonances

NH	**1**		**2**	
	Major	Minor	Major	Minor
Tyr[2]	8.6	8.3	8.0	7.5
Ile[3]	5.5	—	7.5	3.6
Gln[4]	2.5	—	3.6	2.7
Asn[5]	6.4	—	6.0	6.4
Pen[6]	1.3	—	4.0	3.6
Leu[8]	10.2	7.8	6.5	4.5
Gly[9]	7.3	8.8	7.7	8.7

At pH ≈ 3 in 9 : 1 H_2O : D_2O; units of ppm/K × -10^3. — , not observed.

Because of a conformational change observed by CD spectroscopy when switching solvents from water to TFE (see CD section below), NMR spectra of **1** were recorded in TFE-d_2; however, the solubility of **1** in neat TFE did not permit concentrations required for NMR spectroscopy on our 600 MHz instrument. Instead, the peptide was soluble at practical concentrations for NMR experiments in a mixture of 7 : 3 TFE : H_2O. In these conditions the amide protons of Tyr[2], Ile[3], Leu[8] and Gly[9] all shifted significantly upfield ($\Delta\delta$ of 0.7, 0.2, 0.6 and 0.4 ppm, respectively) relative to water (Table 6) indicating a modification of the peptide conformation in changing from water to 7 : 3 TFE : H_2O. In the spectrum of OT (**3**), similar upfield shifts of the amide protons of Ile[3], Leu[8] and Gly[9] have been observed upon the titration of TFE into DMSO [49–51].

Analysis of 1 and 2 with Laser Raman Spectroscopy

Raman spectroscopy has been used to examine the conformation of oxytocin analogs [52–54]. Detailed investigations of disulfide containing molecules with Raman spectroscopy have provided carbon-sulfur, sulfur-sulfur, and amide stretching frequencies for the assignment of specific conformations [55–57]. For example, OT (**3**) and [Gly[4]]-OT, which have been shown

Table 6 Proton NMR Data for [dPen^1, Pen^6]-OT Recorded in 7 : 3 TFE : H_2O

Residue	δ (ppm)[a]	Residue	δ (ppm)
dPen^1		Pen^6	
$C_\alpha H$	2.52	NH	7.69
$C_\alpha H$	2.43	$C_\alpha H$	4.73
$C_\gamma H_3$	1.37	$C_\gamma CH_3$	1.43
$C_\gamma H_3$	1.37	$C_\gamma CH_3$	1.37
		J_{NHCH}	7.1
Tyr^2			
NH	7.58	Pro^7	
$C_\alpha H$	4.53	$C_\alpha H$	4.47
$C_\beta H$	3.15	$C_\beta H$	2.22
$C_\beta H$	3.09	$C_\beta H$	2.07
$C_m H$	7.16	$C_\gamma H$	2.01
$C_o H$	6.86	$C_\gamma H$	2.01
$J_{\delta\varepsilon}$	8.6	$C_\delta H$	3.91
J_{NHCH}	6.6	$C_\delta H$	3.69
Ile^3		Leu^8	
NH	7.51	NH	7.73
$C_\alpha H$	4.12	$C_\alpha H$	4.30
$C_\beta H$	2.04	$C_\beta H$	1.68
$C_\gamma CH_2$	—	$C_\beta H$	1.62
$C_\gamma CH_3$	1.13	$C_\delta H_3$	0.94
$C_\delta CH_3$	0.92	$C_\delta H_3$	0.90
J_{NHCH}	5.8	J_{NHCH}	6.6
Gln^4		Gly^9	
NH	7.76	NH	7.94
$C_\alpha H$	4.19	$C_\alpha H$	3.94
$C_\beta H$	2.16	$C_\alpha H$	3.86
$C_\beta H$	2.16	J_{NHCH}	—
$C_\gamma H$	2.37		
$C_\gamma H$	2.37		
J_{NHCH}	5.6		
Asn^5			
NH	8.34		
$C_\alpha H$	4.82		
$C_\beta H$	2.84		
$C_\beta H$	2.76		
J_{NHCH}	—		

[a] Major isomer; — , not observed.

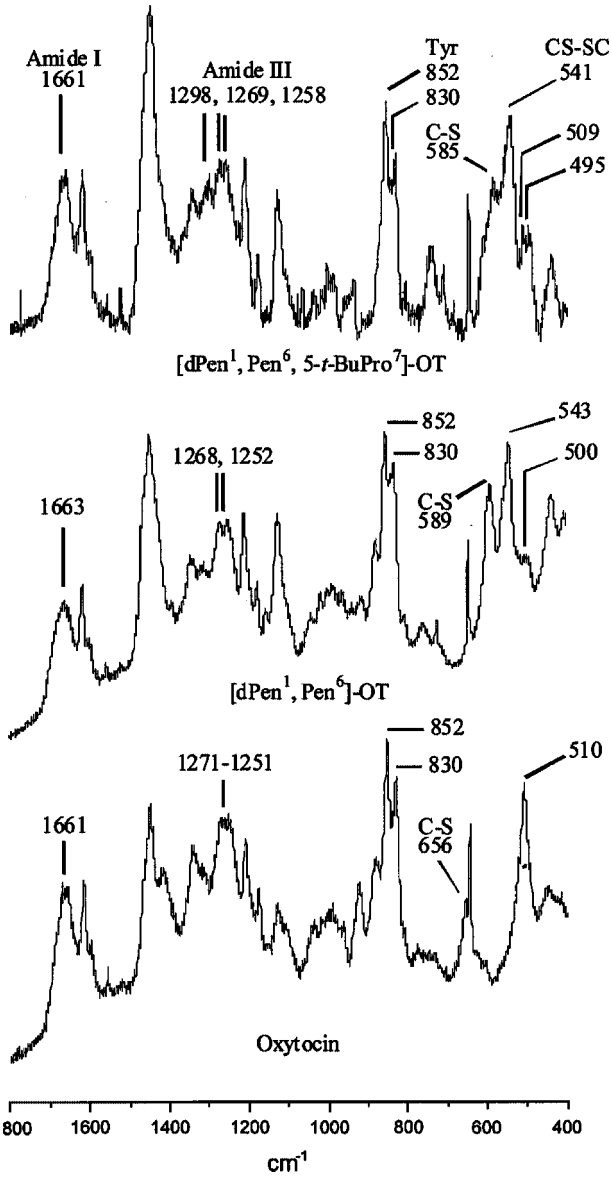

Figure 4 Laser Raman spectra of OT, **1** and **2**.

by NMR spectroscopy to adopt reverse turn structures, exhibit amide I bands at 1663 to 1670 cm^{-1}, resulting from the coupled in-plane stretching vibrations of the amide carbonyl group, as well as amide III bands at 1266 to 1270 cm^{-1}, resulting from the in-plane vibration of the amide bond [53]. Correlation between S-S stretching frequencies and disulfide dihedral angles (χ_{SS-CC} and χ_{CS-SC}) for several alkyl disulfides (primary, secondary, tertiary and strained disulfides) has been established based on the analysis of compounds for which the disulfide geometry was assigned by other means of determination (x-ray crystallography and NMR spectroscopy) [57–60].

In the present study of **1** and **2**, background fluorescence, especially at shorter wavelengths (i.e. the blue 488 nm or the green 515 nm lines of argon), was observed for all of the analogs tested. A longer wavelength (near infrared 782 nm) was used to reduce fluorescence; however, longer acquisition times were required to obtain an acceptable signal to noise ratio. As a reference standard, Raman spectra were first obtained on OT (**3**) and were found to be comparable to literature examples for OT (**3**), the agonist [Gly^4]-OT and the partial agonist [D-Tyr^2]-OT (obtained at 515 nm) [53]. Oxytocin, as well as the analogs **1** and **2**, exhibited similar Tyr (830 and 852 cm^{-1}), amide I (1663 cm^{-1}) and amide III (1251–1271 cm^{-1}) bands, the latter having been associated with β-turns in peptides [52, 53].

The strong disulfide band at 510 cm^{-1} exhibited in the spectrum for OT (**3**) has been shown to be in accordance with a $\pm 90^\circ$ χ_{CS-SC} dihedral angle

(within 30 degrees of ±90°) [52–54]. The antagonist analogs [dPen^1,Pen^6]-OT (**1**) and [dPen^1,Pen^6,5-*t*BuPro^7]-OT (**2**) both exhibited a medium intensity band, at 543 cm^{-1} and 541 cm^{-1}, respectively, which corresponded well with values previously reported for the antagonists [Pen^1]-OT, [Pen^1,Leu^2]-OT, [Pen^1,Thr^4]-OT and [Pen^1,Thr^4]-OT which have been suggested to adopt a 115° χ_{CS-SC} dihedral angle [52,53]. This medium intensity band was assigned to a 115° χ_{CS-SC} dihedral angle based on the x-ray structure of penicillamine disulfide [52,59,61]; however, compounds with alternative χ_{CS-SC} dihedral angle values have exhibited bands around 540 cm^{-1} in their Raman spectra [59,60]. For example, diphenyl disulfide which possesses a χ_{CS-SC} dihedral angle of 84° in its x-ray structure exhibited a strong disulfide stretch at 542 cm^{-1} in the solid state [59]. Because di-*tert*-butyl disulfide exhibited stretches at 540 cm^{-1} (strong) and 507 cm^{-1} (weak) similar to those measured for peptide **2** (Figure 4) [59], the position of the disulfide stretches in the Raman spectra of these tertiary disulfides may be in part indicative of substitution at the β-carbons [59,60]. Additional weaker bands at 509 cm^{-1} and 495 cm^{-1} were also observed in the Raman spectra of **2**. Such closely lying bands near 500 cm^{-1} have been ascribed to a disulfide dihedral angle close to ±90° [57]. Moreover, the C_β-S stretch varied from 585 cm^{-1} to 589 cm^{-1} to 656 cm^{-1} in the respective spectra of peptides **2, 1**, and OT, and was characteristic of the differences between tertiary and primary disulfides [58].

Analysis of 1 and 2 by Circular Dichroism Spectroscopy

Specific peptide conformations exhibit characteristic CD spectra [62–64]. Because oxytocin analogs possess chromophores, such as the tyrosine aromatic ring, the disulfide bond and amide bonds, CD has been used to study the conformation of agonists and antagonists [52–54, 65–68]. In particular, CD provides a convenient means for studying the influence of environment on peptide conformation. For this reason, the CD spectra of analogs **1** and **2** were measured in water, methanol, acetonitrile and 2,2,2-trifluoroethanol (TFE) to examine the influence of environment on conformation.

The general appearance of the spectra of **1** was similar in water, methanol and acetonitrile exhibiting a shallow negative maximum around 270–279 nm ([θ] = −780, −1298, and −996, respectively) and a positive maximum at 229–234 nm ([θ] = 5439, 7010 and 3773, respectively, Figure 5). On the other hand, in TFE, the CD spectrum of **1** changed shape and exhibited a shallow negative maximum at 274 nm ([θ] = −1254) and a second negative maximum at 240 nm, [θ] = −2034. The general appearance of the CD spectra of **2** remained relatively similar in all four solvents exhibiting a strong negative maximum at 236–239 nm (Figure 6); moreover, the intensity of this maximum augmented in TFE (from [θ] = −16 200−−18 060 to [θ] = −23 900).

Although the assignment of these bands may be complicated because of their potential association with the tyrosine aromatic residue and the disulfide bond, significant evidence exists to suggest that the contribution of the former is less important in the 230–250 nm region of the CD spectra measured at neutral pH. Titration studies of oxytocin analogs have indicated that ionization (at pH 10.4) of the tyrosine hydroxyl generates a positive band at 240 nm in the CD spectrum of [Pen^1]-OT; however, this band was not present at neutral nor acid pH, nor in the spectra of [Pen^1,Leu^2]-OT (without the Tyr^2 residue) at different pH values [52]. Furthermore, spectra of OT analogs without disulfides do not exhibit CD bands in the 230–250 nm region at 20 °C and neutral pH [68]. Peptides having disulfide bonds and no aromatic residues have shown bands around 240 nm in their CD spectra [69,70]. For example, the CD spectra of D-penicillamine mixed ethyl disulfide (D-PenS-SCH_2CH_3) in methanol exhibits a positive maximum around 238 nm [71]. Conformationally restricted disulfides

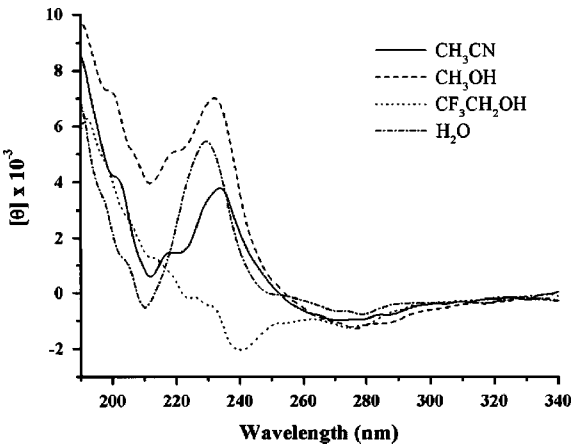

Figure 5 CD spectra of [dPen^1,Pen^6]-OT **1**.

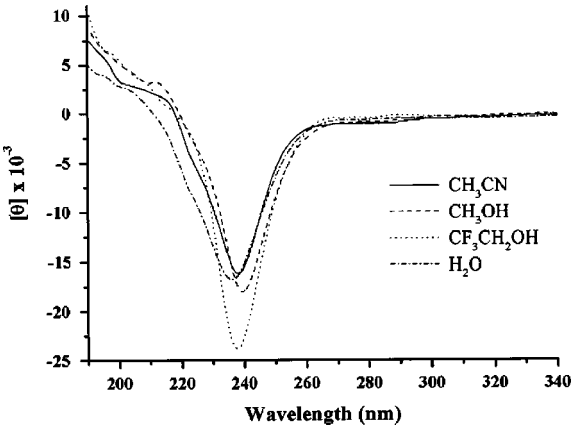

Figure 6 CD spectra of [dPen^1,Pen^6,5-*t*BuPro^7]-OT **2**.

exhibit strong CD bands in this region [65,69,70,72,73]. For example, in their respective CD spectra in TFE, malformin A_1 **5** (Figure 1), which possesses a D-Cys-D-Cys strained disulfide, exhibited a strong positive maximum at around 235 nm [69], its enantio-[5-valine]malformin analogue with L-Cys disulfide showed a negative maximum at the same wavelength [70], and desthiomalformin without the disulfide, having D-Ala in place of D-Cys, exhibited no such band [74].

In the CD spectra of disulfides, two maxima of opposite sign were generally observed, one being referred to as the long wavelength (>250 nm) or low energy transition and the other as the shorter wavelength (<250 nm) or higher energy transition. Application of the Bergson model for determination of disulfide chirality has correlated disulfide geometry with optical activity, Cotton effect amplitude and the location of disulfide bands in the CD spectra [75,76]. In particular, the magnitude of the long wavelength transition varies with geometry and follows the quadrant rule (Figure 2) [75,77]. In the case of disulfides with right-handed screw sense (*P*-helicity) having dihedral angles of $0^\circ < \chi_{CS-SC} < 90^\circ$ the long wavelength CD band is positive. Conversely, the long wavelength transition is negative for disulfides dihedral angles of $90^\circ < \chi_{CS-SC} < 180^\circ$ (*P*-helicity). For a χ_{CS-SC} value of 90°, the long wavelength transition is not observed because of degeneracy [75,76]. This correlation has been verified primarily with molecules and peptides containing primary disulfides for which specific CD patterns were predicted based on different disulfide dihedral angle geometry.

In the CD spectra of **1**, the shallow negative maximum at 270–279 nm corresponded to a long wavelength disulfide transition (with a possible contribution from transitions of the Tyr^2 phenolate). In water, methanol and acetonitrile, the spectra for **1** also exhibited a positive maximum corresponding to the shorter wavelength transition of the disulfide. Interpretation of the CD spectra for **1** in these three solvents according to the Bergson model leads to either a right-handed screw sense (*P*-helicity, Figure 2) with a χ_{CS-SC} dihedral angle value of close to +115° or a left-handed screw sense (*M*-helicity, Figure 2) with a χ_{CS-SC} dihedral angle of around −60°. The former value (+115°) has previously been ascribed to [Pen^1, Leu^2]-OT which possesses a mixed tertiary-primary disulfide and exhibits a negative longer wavelength transition at 276–279 nm and a positive shorter wavelength disulfide band at 248 nm [52]. The latter value (−60°) is rare in macrocyclic disulfides and likely to be disfavored due to the steric interaction of the substituted β-carbons of the mixed deamino-penicillamine-L-penicillamine disulfide [52]. However, such a conformation ($\chi_{CS-SC} = -60^\circ$) has been proposed for malformin A_1 **5** (Figure 1), which possesses a strained cyclic disulfide, and exhibits CD spectra with a strong positive maximum at 235 nm and a negative maximum at 280 nm [69,71]. To the best of our knowledge, no extensive CD study of di-tertiary disulfides ($R_3CS\text{-}SCR_3$) has been reported;[¶] however, further support for our assignment can be inferred from the study of D-penicillamine disulfide which showed a χ_{CS-SC} dihedral angle of +115° in its x-ray structure [61], and exhibited a 543 cm^{-1} disulfide stretch in its Raman spectra, comparable to the 543 cm^{-1} disulfide stretch seen in the Raman spectra of **1** (Figure 4) [59].

The CD spectra of analog **2** exhibited a strong negative maximum at 236–239 nm. Because no long wavelength contribution was detected, the disulfide χ_{CS-SC} dihedral angle was assigned to a value of ±90° [76,78]. Although the assignment of the screw sense of the disulfide can not be made based solely on the shorter wavelength transition [54,72,75,76,78], indirect evidence to suggest a right-handed screw sense (*P*-helicity) comes from the CD spectra of *cyclo*-L-cystine which was shown by NMR spectroscopy to adopt a χ_{CS-SC} dihedral angle of +90°. A strong negative Cotton effect at 228 nm that was correlated to *P*-helicity was observed in the CD spectra for this strained diketopiperazine in ethanol and assigned to a perturbed peptide $n \rightarrow \pi^*$ transition [78].

The CD spectrum for **1** in TFE could not be assigned to a single conformation, because of the presence of two shallow negative maxima at 274 nm and 240 nm. A change in conformation about the disulfide bond was indicated by the disappearance of the positive maximum around 229–234 nm and the appearance of a negative maximum at 240 nm in going from water to TFE as solvent. The TFE spectrum for **1** may result from contributions of two conformers in equilibrium about the disulfide [65]: one having a $+115^\circ \chi_{CS-SC}$ dihedral angle and *P*-helicity as described for **1** in water, and the other having a $\pm 90^\circ \chi_{CS-SC}$ dihedral angle exhibiting no contribution in the long-wavelength region and a strong negative contribution in the short wavelength region as described for compound **2**. This composite CD spectrum would exhibit two shallow negative maxima, one in the long wavelength region, and one in the short wavelength region, as observed in the CD spectra for **1** in TFE. Similar composite spectra have been assigned to the retro-D analog of tocinamide **6** (Figure 1), whose CD spectra were compatible with a combination of +115° and $-60^\circ \chi_{CS-SC}$ dihedral angles [65].

Analysis of 1 and 2 by Molecular Modeling

Although the NMR spectra suggested that analogs **1** and **2** were conformationally flexible in aqueous solution, the presence of some inter-residue NOEs in

[¶] Relevant examples of CD include the spectra of D-penicillamine disulfide and mixed ethyl-D-penicillamine are reported in reference [71]. The absorption spectra of di-*tert*-butyl disulfide and related alkyl disulfides are reported in reference [89]. For Raman spectra of tertiary disulfides see references [58–60].

the major (*trans*-) conformers of **1** and **2** suggested along with the Raman and CD data that a subset of lower-energy conformations existed with a specific disulfide geometry. Computational methods have been used extensively to search for preferred conformations for oxytocin analogs, and have resulted in the discovery of several families of stable conformations [23,79–83]. In a similar fashion, a conformational search was undertaken to assess whether or not the observed data corresponded to a unique set of conformations for both analogs. Initial Monte Carlo conformational searches [37,39] were performed on both the *trans*- and *cis*-conformers of **1** and **2**, but failed to converge to low energy structures. Extensive Monte Carlo conformational searches were also conducted using distance restraints derived from the observed inter-residue NOEs for the major (*trans*-) conformers of **1** and **2**. Searches on both analogs converged to families of low energy conformations in the presence of restraints. No similar searches were done on the minor (*cis*-) conformers owing to a paucity of inter-residue NOEs, and thus an absence of potential restraints.

For analog **1**, two families of expanded conformations (**1**^{a} and **1**^{b}), emerged from the search in a 2 : 1 ratio (Figure 7). The lowest energy set (−1324 kJ/mol) of conformations, **1**^{a}, possesses two reverse turns, one centered on Gln^{4}-Asn^{5} (Type VIII beta turn, ϕ^{4} −49.6°, ψ^{4} −53.0°, ϕ^{5} −147.3°, ψ^{5} 140.0°) and the second centered on Pro^{7}-Leu^{8} (ϕ^{7} −74.3°, ψ^{7} 51.0°, ϕ^{8} −134°, ψ^{8} −64.9°). A similar Gln^{4}-Asn^{5} reverse turn has been observed as a major conformer for the potent antagonist [dPen^{1},*cyclo*(Glu^{4},Lys^{8})]-OT (pA$_{2}$ 8.74) [84]. This family of conformations appears stabilized by a multipoint hydrogen bond between the Gly^{9} terminal amide, the Asn^{5} sidechain, the Pen^{6} carbonyl and the Pen^{6} amide nitrogen. In addition, hydrophobic packing is observed between the geminal dimethyls of Pen^{6}, the sidechain of Leu^{8}, and the phenolic ring of Tyr^{2}. In most conformations, an additional hydrogen bond appears between the sidechain and backbone amide of Gln^{4}. The observed disulfide dihedral angle clusters around +114° (P helicity). The observed backbone ϕ dihedral angles also closely fit the calculated values from the $^{3}J_{NH-H\alpha}$ coupling constants (Table 2). A similar conformation has been calculated to be one of the two lowest energy conformers of OT (**3**) [80].

Table 7 Calculated Free Energies for **1** and **2**

Analog	Conformer	Force field	Restraints	E (kJ/mol)
1	Major/*trans*	AMBER*	No	−1028.7
2	Major/*trans*	AMBER*	No	−1025.9
1^{a}	Major/*trans*	OPLS-AA	Yes	−1324.0
1^{b}	Major/*trans*	OPLS-AA	Yes	−1315.3
2	Major/*trans*	OPLS-AA	Yes	−1203

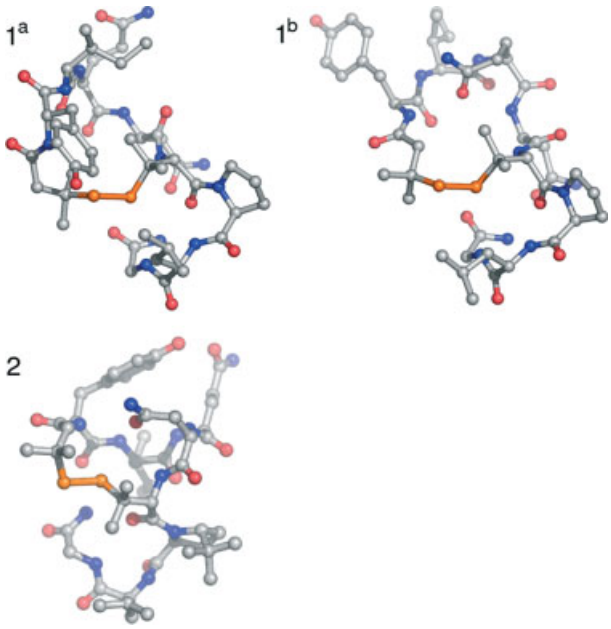

Figure 7 Low energy conformations of analogs **1** and **2**. Images generated using PyMOL [43].

The higher energy (−1315 kJ/mol) set of conformations, **1**^{b}, possesses a similar reverse turn at Pro^{7}-Leu^{8} (ϕ^{7} −73.3°, ψ^{7} 58.9°, ϕ^{8} −150.1°, ψ^{8} −66.7°), and a tighter structure, resulting in a relatively close distance between the amide NH of Tyr^{2} and Asn^{5} (3.15 Å), arising from a three-point hydrogen bond formed with the sidechain of Gln^{4}, as well as a short distance between the C$_{\alpha}$H of Asn^{5} and the NH of Pen^{6} (2.18 Å). The observed disulfide dihedral angle clusters around +116° (P helicity). The observed backbone ϕ dihedral angles for **1**^{b} also closely fit the calculated values from the $^{3}J_{NH-H\alpha}$ coupling constants for residues Tyr^{2}, Ile^{3}, Pen^{6}, Pro^{7} and Leu^{8} (Table 2). The backbone dihedral angles of Asn^{5} are outlying on a Ramachandran plot (ϕ^{5}81°,ψ^{5}92°). Taken together, both sets of conformations (**1**^{a} and **1**^{b}) are consistent with the observed NOEs and solvent shielding data for the major conformer of **1**, as well as the observed CD and Raman spectra.

For analog **2**, one family of compact conformations was found at a higher energy (−1203 kJ/mol) than either family of conformations for analog **1** (Figure 7). In this set of conformations, the phenolic ring of Tyr^{2} is packed over the macrolide cycle, partially stabilized by a putative hydrogen bond between the phenol and the sidechain of Gln^{4}. The *tert*-butyl group of *t*-BuPro^{7} is packed tightly against the geminal dimethyls of Pen^{6} and the Leu^{8} sidechain, which places the C$_{\alpha}$H of Pen^{6} close to the C$_{\delta}$H and C$_{\delta}$*t*Bu of 5-*t*BuPro^{7}. The sidechain of Asn^{5} rests in the center of the peptide cycle, below the ring of Tyr^{2}, and forms a putative four-point hydrogen bond with the backbone amide protons of Tyr^{2}, Ile^{3} and Pen^{6}. The terminal amide of Gly^{9} also makes a putative three-point hydrogen bond with the backbone carbonyl of Tyr^{2} and Pen^{6}. The

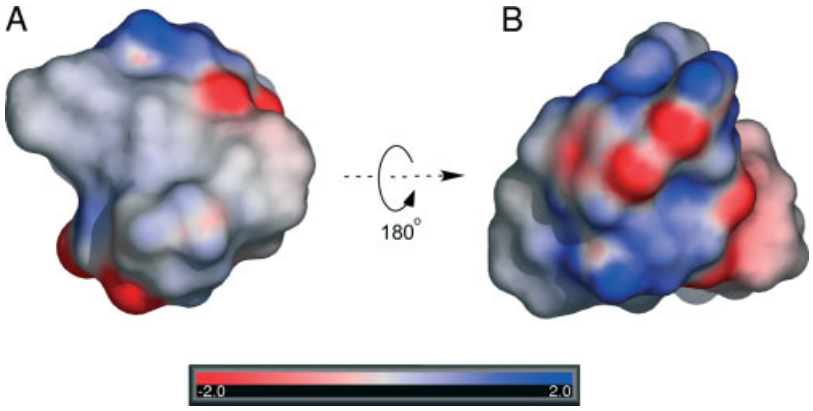

Figure 8 Electrostatic potential of the lowest energy conformation of **2** mapped onto the surface. **A**. Conformation of **2** from the same perspective as Figure 7. The hydrophobic patch is clearly visible. Rotating the molecule by 180° results in **B**, showing the charge distribution on the other side of the molecule. This image was generated using APBS [40] and PyMOL [43].

observed disulfide dihedral angle clusters around +104° (P helicity). The observed backbone ϕ dihedral angles also closely fit the calculated values from the $^3J_{NH-H\alpha}$ coupling constants (Table 3). The backbone dihedral angles of Ile^3 are outlying on a Ramachandran plot (ϕ^5 −161°, ψ^5 −51°). This structure for **2** matches with the existing Raman and CD observations, and results in opposing hydrophilic and hydrophobic faces (Figure 8).

The changes in the electrostatic environment and ellipticity that were measured for **1** upon changing solvents from water to 7:3 TFE:H_2O may also be explained if analog **1** adopted a similar conformation as shown for **2**. Such a relatively compacted structure would be expected to have an increase in observable long-range inter-residue NOEs, although the higher energy of the stable conformations of **2** compared with **1** suggests that this conformation would be less frequently populated in aqueous solution for **1** than for **2**.

An interesting comparison can be made between the conformation of **2** and conformations previously found in a comprehensive molecular dynamics study of [Mpa^1,*cyclo*(Glu^4,Lys^8)]-OT and [dPen^1,*cyclo*(Glu^4,Lys^8)]-OT [23], using distance restraints derived from NMR studies in DMSO. The additional lactam bridge between residues 4 and 8 on these analogs was shown to constrain the geometry of the three residue exocyclic 'tail' of oxytocin, such that they adopted conformers with a similar amphipathic character as **2**. A polar surface was formed by backbone amides and the sidechains of Tyr^2 and Asn^5. A hydrophobic patch was composed of the sidechains of Mpa^1(dPen^1),Tyr^2, Ile^3, Cys^6, Pro^7 and Lys^8. In [dPen^1,*cyclo*(Glu^4,Lys^8)]-OT, resulted in a continuous hydrophobic surface [23], similar that observed for **2**.

CONCLUSIONS

Although the NMR data suggested considerable conformational flexibility about the different side-chains for peptides **1** and **2**, the Raman and CD spectra indicated preferred conformations for the disulfide geometry of these analogs, which were reinforced by a Monte Carlo conformational search that found several families of low energy conformations for **1** and **2**. The observed CD spectra for **1** in water, acetonitrile and methanol corresponded well with a χ_{CS-SC} dihedral angle of +115° and *P*-helicity; however, the spectra for **1** in TFE shifted to suggest two different disulfide conformers possessing ±90° and +115° χ_{CS-SC} dihedral angles. The CD spectra of **2** in all solvents were indicative of a χ_{CS-SC} dihedral angle closer to ±90° because no long wavelength disulfide contribution was observed. The *tert*-butyl group and the disulfide were shown to be in close proximity by the presence of a strong NOE between $C_\alpha H$ of Pen^6 and the *tert*-butyl group of 5-*t*BuPro^7 in the NMR spectra for **2**. Steric repulsion between the *tert*-butyl group on proline at position 7 and the β-methyl groups on penicillamine at position 6 appeared to favor a particular conformation close to ±90° about the disulfide in **2**. Two rotations about the disulfide could explain the conformational change for analog **1**: one going from +115° to +90°, and the other passing from +115° to −90°. Conformational analysis using a Monte Carlo conformational search using restraints generated from observable NOEs further supported that **2** adopts a stable, compacted conformation with a χ_{CS-SC} dihedral angle of +104°, suggesting that the dominant conformational transition observed is the former.

Analogs **1** and **2** differ solely because of the presence of the (5*R*)-*tert*-butyl substituent on Pro^7. Significant differences in their conformations and in their dynamic properties beyond disulfide geometry were, however, apparent from the present study. For example, a lower barrier for isomerization about the amide *N*-terminal to the 5-*tert*-butylproline residue was measured in **2** relative to proline-containing analogs of OT (approximately 4 kcal/mol lower). An increased prolyl amide *cis*-isomer population was

also measured for *tert*-butyl analog **2**. Although both analogs are conformationally flexible about the prolyl *N*-terminal amide bond, they may adopt different predominant conformations when bound at the receptor. Because the significant increase in *cis*-isomer population for **2** over **1** did not correspond to an increase in antagonistic activity (EC_{50} values for **1** and **2** are 6.0 and 6.5 nM, respectively), the absence of *cis*-prolyl amide geometry does not correlate with reduced binding and antagonism within these analogs, unlike the rigid (and similarly potent) antagonists [Mpa^1,cyclo(Glu^4,Lys^8)]-OT and [dPen^1,cyclo(Glu^4,Lys^8)]-OT which possess a *cis*-prolyl amide geometry [23,24,85,86]. Because the disulfide geometry of **2** was not affected by changes in environment, a χ_{CS-SC} dihedral angle near $+90^\circ$ may be a prerequisite for both analogs to bind at the OT receptor.

Considering that the minimum energy conformation obtained from computational analysis of analog **2** is relevant for binding at the receptor, and analog **1** adopts a similar conformation, then the data for **1** and **2** support the 'cooperative' model for oxytocin binding [16]. In the 'cooperative' model, oxytocin analogs adopt conformations that place the hydrophilic and hydrophobic residues on opposite faces of the molecule. Binding is promoted by hydrophobic interactions between the receptor and a hydrophobic surface formed by the sidechains of Ile^3, Gln^4, Pro^7 and Leu^8. Such an amphipathic structure is observed in the minimum energy conformer of analog **2** (Figure 8). Moreover, because of the presence of the 5-*t*BuPro, analog **2** is more hydrophobic than **1** and exhibits a slightly higher receptor affinity *in vitro* ($K_i = 33$ nM for **2** vs 37 nM for **1**).

In contrast to the 'dynamic' model, which postulates that conformationally rigid OT analogs should prove better at binding to the uterine receptor [17,18], analogs **1** and **2** are both substantially more flexible (and less structured) than native OT (**3**) yet both exhibit similar binding and antagonistic activity as the most constrained OT analogs. The 'dynamic' model does predict that antagonists bind in a different conformation than OT (**3**), and that antagonists may prevent the conversion of oxytocin analogs from an initial bound conformation to a final conformation that allows for signal transduction. In accordance with the dynamic model, the constrained disulfide geometry around [dPen^1,Pen^6], and the increased hydrophobicity from the β-methyl groups on [dPen^1,Pen^6] and *tert*-butyl group on *t*BuPro^7 may stabilize a specific binding conformation for analogs **1** and **2** at the receptor [87]. This work demonstrated, furthermore, that hydrophobic effects of added methyl substituents may stabilize the receptor bound conformation as effectively as structural constraints that bridge regions of the peptide.

Acknowledgements

This research was supported in part by the Natural Sciences and Engineering Research Council of Canada, Valorisation Recherche Québec and the Ministère de l'Éducation du Québec. We thank Sylvie Bilodeau and Dr M. T. Phan Viet of the Regional High-Field NMR Laboratory for their assistance. We are grateful to Professor Tom Ellis of the Materials Characterization Laboratory at the Université de Montréal and to Dr Samir Elouatik for conducting the Raman experiments. We are thankful to Professor Joanne Turnbull and her group at Concordia University for use of the CD spectropolarimeter.

REFERENCES

1. Marshall GR. Peptide interactions with G-protein coupled receptors. *J. Peptide Sci.* 2001; **60**: 246–277.
2. Hruby VJ. Relation of conformation to biological activity in oxytocin, vasopressin and their analogues. In *Topics in Molecular Pharmacology*, Burgen ASV, Roberts GCK (eds). Elsevier: Amsterdam, 1981; 99–126.
3. Hruby VJ, Chow M-S, Smith DD. Conformational and structural considerations in oxytocin-receptor binding and biological activity. *Annu. Rev. Pharmacol. Toxicol.* 1990; **30**: 501–534.
4. Manning M, Stoev S, Cheng LL, Wo NC, Chan WY. Design of oxytocin antagonists which are more selective than atosiban. *J. Peptide Sci.* 2001; **7**: 449–465.
5. Hruby VJ, Smith CW. In *Chemistry, Biology, and Medicine of Neurohypophyseal Hormones and Their Analogs*, Smith CW (ed.). Vol. 8. Academic Press: Orlando, 1987; 77–207.
6. Jost K, Lebl M, Brtnik F (eds). *CRC Handbook of Neurohypophyseal Hormone Analogs*, Vol. 2. CRC Press: Boca Raton, FL, 1987.
7. du Vigneaud V, Ressler C, Swan JM, Roberts CW, Katsoyannis PG, Gordon S. The synthesis of an octapeptide amide with the hormonal activity of oxytocin. *J. Am. Chem. Soc.* 1953; **75**: 4879–4880.
8. du Vigneaud V, Lawler HC, Popenoe EA. Enzymatic cleavage of glycinamide from vasopressin and a proposed structure for this pressor-antidiuretic hormone of the posterior pituitary. *J. Am. Chem. Soc.* 1953; **75**: 4880–4881.
9. López-Zeno JA, Peaceman AM, Adashek JA, Socol ML. A controlled trial of a program for the active management of labor. *N. Engl. J. Med.* 1992; **326**: 450–454.
10. Åkerlund M, Strömberg P, Hauksson A, Andersen LF, Lyndrup J, Trojnar J, Melin P. Inhibition of uterine contractions of premature labor with an oxytocin analogue. Results from a pilot study. *Br. J. Obstet. Gynaecol.* 1987; **84**: 1040–1044.
11. Andersen LF, Lyndrup J, Akerlund M, Melin P. Oxytocin receptor blockade: a new principle in the treatment of preterm labor? *Am. J. Perinatol.* 1989; **6**: 196–199.
12. Wilson L, Jr, Parsons MT, Flouret G. Inhibition of spontaneous uterine contractions during the last trimester in pregnant baboons by an oxytocin antagonist. *Am. J. Obstet. Gynecol.* 1990; **163**: 1875–1882.
13. Evans BE, Leighton JL, Rittle KE, Gilbert KF, Lundell GF, Gould NP, Hobbs DW, DiPardo RM, Veber DF, Pettibone DJ, Clineschmidt BV, Anderson PS, Freidinger RM. Orally active, nonpeptide oxytocin antagonists. *J. Med. Chem.* 1992; **35**: 3919–3927.
14. Melin P, Trojnar J, Johansson B, Vilhardt H, Akerlund M. Synthetic antagonists of the myometrial response to vasopressin and oxytocin. *J. Endocrinol.* 1986; **111**: 125–131.
15. Walter R. Conformations of oxytocin and lysine-vasopressin and their relationships to the biology of neurohypophyseal hormones.

In *Structure-Activity Relationships of Protein and Polypeptide Hormones*, Margoulies M, Greenwood FC (eds). Excerpta Medica Foundation: Amsterdam, 1971; 181–193.
16. Walter R. Identification of sites in oxytocin involved in uterine receptor recognition and activation. *Fed. Proc.* 1977; **36**: 1872–1878.
17. Meraldi J-P, Hruby VJ, Brewster ARI. Relative conformational rigidity in oxytocin and [1-penicillamine]-oxytocin: A proposal for the relationship of conformational flexibility to peptide hormone agonism and antagonism. *Proc. Natl Acad. Sci. USA* 1977; **74**: 1373–1377.
18. Hruby VJ. Structure and conformation related to the activity of peptide hormones. In *Perspectives in Peptide Chemistry*, Eberle A, Geiger R, Wieland T (eds). Karger: Basel, 1981; 207–220.
19. Wood SP, Tickle IJ, Treharne AM, Pitts JE, Mascarenhas Y, Li JY, Husain J, Cooper S, Blundell TL, Hruby VJ, Buku A, Fishman AJ, Wyssbrod HR. Crystal structure analysis of deamino-oxytocin: Conformational flexibility and receptor binding. *Science* 1986; **232**: 633–636.
20. Hruby VJ. Implications of the x-ray structure of deamino-oxytocin to agonist/antagonist-receptor interactions. *Trends Pharm. Sci.* 1987; **8**: 336–339.
21. Larive CK, Guerra L, Rabenstein DL. *Cis/trans* conformational equilibrium across the cysteine(6)-proline peptide bond of oxytocin, arginine vasopressin, and lysine vasopressin. *J. Am. Chem. Soc.* 1992; **114**: 7331–7337.
22. Larive CK, Rabenstein DL. Dynamics of *cis/trans* isomerization of the cysteine(6)-proline peptide bonds of oxytocin and arginine-vasopressin in aqueous and methanol solutions. *J. Am. Chem. Soc.* 1993; **115**: 2833–2836.
23. Shenderovich M, Wilke S, Kövér KE, Wilke S, Collins N, Hruby VJ. Solution conformations of potent bicyclic antagonists of oxytocin by nuclear magnetic resonance spectroscopy and molecular dynamics simulations. *J. Am. Chem. Soc.* 1997; **119**: 5833–5846.
24. Shenderovich M, Wilke S, Kövér KE, Collins N, Hruby VJ, Liwo A, Ciarkowski J. Solution conformation of a potent bicyclic antagonist of oxytocin. *Polish J. Chem.* 1994; **68**: 921–927.
25. Bélec L, Maletinska L, Slaninová J, Lubell WD. The influence of steric interactions on the conformation and biology of oxytocin. Synthesis and analysis of penicillamine^{6}-5-tert-butylproline^{7}-oxytocin analogues. *J. Pept. Res.* 2001; **58**: 263–273.
26. Wüthrich K. In *NMR of Proteins and Nucleic Acids*. John Wiley & Sons, Inc: New York, 1986; 117–175.
27. Ämmälahti E, Bardet M, Molko D, Cadet J. Evaluation of distances from ROESY experiments with the intensity-ratio method. *J. Magn. Res. A* 1996; **122**: 230–232.
28. Mohamadi F, Richards NGJ, Guida WC, Liskamp R, Lipton M, Caufield C, Chang G, Hendrickson T, Still WC. Macromodel: an integrated software system for modeling organic and bioorganic molecules using molecular mechanics. *J. Comp. Chem.* 1990; **11**: 440.
29. Still WC, Tempczyk A, Hawley RC, Hendrickson T. Semianalytical treatment of solvation for molecular mechanics and dynamics. *J. Am. Chem. Soc.* 1990; **112**: 6127–6129.
30. Qiu D, Shenkin PS, Hollinger FP, Still WC. The GB/SA continuum model for solvation. A fast analytical method for the calculation of approximate born radii. *J. Phys. Chem. A* 1997; **101**: 3005–3014.
31. Weiner SJ, Kollman PA, Case DA, Singh UC, Ghio C, Alagona G, Profeta S, Weiner P. A new force field for molecular mechanical simulation of nucleic acids and proteins. *J. Am. Chem. Soc.* 1984; **106**: 765–784.
32. Weiner SJ, Kollman PA, Nguyen DT, Case DA. An all atom force field for simulations of proteins and nucleic acids. *J. Comp. Chem.* 1986; **7**: 230–252.
33. Ferguson DM, Kollman PA. Can the Lennard-Jones 6–12 function replace the 10–12 form in molecular mechanics calculations? *J. Comp. Chem.* 1991; **12**: 620–626.
34. Jorgensen WL, Maxwell DS, Tirado-Rives J. Development and testing of the OPLS all-atom force field on conformational energetics and properties of organic liquids. *J. Am. Chem. Soc.* 1996; **118**: 11 225–11 235.
35. Kaminski GA, Friesner RA, Tirado-Rives J, Jorgensen WL. Evaluation and reparametrization of the OPLS-AA force field for proteins via comparison with accurate quantum chemical calculations on peptides. *J. Phys. Chem. B.* 2001; **105**: 6474–6487.
36. Polak E, Ribière G. Note sur la convergence de méthods de directions conjugées. *Revue Française Inf. Rech. Oper.* 1969; **16-R1**: 35–43.
37. Chang G, Guida WC, Still WC. An internal-coordinate Monte Carlo method for searching conformational space. *J. Am. Chem. Soc.* 1989; **111**: 4379–4386.
38. Saunders M, Houk KN, Wu YD, Still WC, Lipton M, Chang G, Guida WC. Conformations of cycloheptadecane. A comparison of methods for conformational searching. *J. Am. Chem. Soc.* 1990; **112**: 1419–1427.
39. Goodman JM, Still WC. A unbounded systematic search of conformational space. *J. Comp. Chem.* 1991; **12**: 1110–1117.
40. Baker NA, Sept D, Joseph S, Holst MJ, McCammon JA. Electrostatics of nanosystems: Application to microtubules and the ribosome. *Proc. Natl Acad. Sci. USA* 2001; **98**: 10 037–10 041.
41. Holst M, Saied F. Multigrid solution of the poisson-Boltzmann equation. *J. Comp. Chem.* 1993; **14**: 105–113.
42. Holst M, Saied F. Numerical solution of the nonlinear Poisson-Boltzmann equation: Developing more robust and efficient methods. *J. Comb. Chem.* 1995; **16**: 337–364.
43. DeLano WL. *The PyMOL Molecular Graphics System*. DeLano Scientific: San Carlos, CA, USA, 2002.
44. Huang Z, He Y-B, Raynor K, Tallent M, Reisine T, Goodman M. Main chain and side chain chiral methylated somatostatin analogs: Syntheses and conformational analyses. *J. Am. Chem. Soc.* 1992; **114**: 9390–9401.
45. Bystrov VF, Ivanov VT, Portnova SL, Balashova TA, Ovchinnikov YA. Refinement of the angular dependence of the peptide vicinal NH-CalphaH coupling constant. *Tetrahedron* 1973; **29**: 873–877.
46. Shenderovich MD, Nikiforovich GV, Chipens GI. Conformational dependence of the local nuclear overhauser effects in peptides. *J. Magn. Reson.* 1984; **59**: 1–12.
47. Beausoleil E, Lubell WD. Steric effects on the amide isomer equilibrium of prolyl peptides. Synthesis and conformational analysis of N-acetyl-5-tert-butylproline N′-methylamides. *J. Am. Chem. Soc.* 1996; **118**: 12 902–12 908.
48. Hruby VJ. In *Chemistry and Biochemistry of Amino Acids, Peptides and Proteins*, Weinstein B (ed.). Marcel Dekker: New York, 1974; 1–170.
49. Urry DW, Ohnishi M, Walter R. Secondary structure of the cyclic moiety of the peptide hormone oxytocin and its deamino analog. *Proc. Natl Acad. Sci. USA* 1970; **66**: 111–116.
50. Urry DW, Walter R. Lysine vasopressin: conformation in solution. *Proc. Natl Acad. Sci. USA* 1971; **68**: 956–958.
51. Walter R, Glickson JD. Proton magnetic resonance study of peptide conformation: Effect of trifluoroethanol on oxytocin and 8-lysine-vasopressin. *Proc. Natl Acad. Sci. USA* 1973; **70**: 1199–1203.
52. Hruby VJ, Deb KK, Fox J, Bjarnason J, Tu AT. Conformational studies of peptide hormones using laser Raman and circular dichroism spectroscopy. A comparative study of oxytocin agonists and antagonists. *J. Biol. Chem.* 1978; **253**: 6060–6067.
53. Hruby VJ, Mosberg HI, Fox JW, Tu AT. Conformational comparisons of oxytocin agonists, partial agonists, and antagonists using laser Raman and circular dichroism spectroscopy. Examination of 1-penicillamine and diastereoisomeric analogues. *J. Biol. Chem.* 1982; **257**: 4916–4924.
54. Maxfield FR, Scheraga HA. A Raman spectroscopic investigation of the disulfide conformation in oxytocin and lysine vasopressin. *Biochemistry* 1977; **16**: 4443–4449.
55. Lagant P, Vergoten G, Thomas GA, Peticolas WL. Normal modes of folded peptides: beta and gamma turns. A critical point of view. In *ICORS XI London '88. International Conference on Raman*

Spectroscopy, Clark RJH, Long DA (eds). John Wiley & Sons: New York, 1988; 119–120.
56. Arêas EPG, Gabilan N, Laure CJ, Kawano Y. Raman spectra of phospholipase A2 from snake toxin (*Crotalus durissus terrificus*). In *ICORS XI London '88. International Conference on Raman Spectroscopy*, Clark RJH, Long DA (eds). John Wiley & Sons, Inc: New York, 1988; 769–770.
57. Freeman SK. In *Applications of Laser Raman Spectroscopy*. John Wiley & Sons, Inc: New York, 1974; 202–242; 258–306.
58. Sugeta H, Go A, Miyazawa T. Vibrational spectra and molecular conformation of dialkyl disulfides. *Bull. Chem. Soc. Japan* 1973; **46**: 3407–3411.
59. Van Wart HE, Scheraga HA. Raman spectra of cystine-related disulfides. Effect of rotational isomerism about carbon-sulfur bonds on sulfur-sulfur stretching frequencies. *J. Phys. Chem.* 1976; **80**: 1812–1823.
60. Van Wart HE, Scheraga HA. Raman spectra of strained disulfides. Effect of rotation about sulfur-sulfur bonds on sulfur-sulfur stretching frequencies. *J. Phys. Chem.* 1976; **80**: 1823–1832.
61. Rosenfeld RE, Jr, Parthasarathy R. Structure and conformation of amino acids containing sulfur. III. The crystal structure and absolute configuration of 3,3,3′,3′-tetramethyl-D-cystine (D-penicillamine disulfide) dihydrochloride: An unusually short intramolecular N-H···S contact distance. *Acta Cryst. B.* 1975; **31**: 462–468.
62. Woody RW. In *Peptides, Polypeptides, and Proteins*, Blout ER, Bovey FA, Goodman M, Lotan N (eds). Wiley: New York, 1974; 338–350.
63. Crabbé P. In *ORD and CD in Chemistry and Biochemistry, An Introduction*. Academic Press: New York, 1972; 54–58.
64. Blout ER. Polypeptides and proteins. In *Fundamental Aspects and Recent Developments in Optical Rotatory Dispersion and Circular Dichroism*, Ciardelli F, Salvadori P (eds). Heyden & Son, Ltd: New York, 1973; 352–372.
65. Kopple KD, Dickinson HR, Nakagawa SH, Flouret G. Solution conformation of a retro-D analogue of tocinamide. *Biochemistry* 1976; **15**: 2945–2952.
66. Beychok S, Breslow E. Circular dichroism of oxytocin and several oxytocin analogues. *J. Biol. Chem.* 1968; **243**: 151–154.
67. Urry DW, Quadrifoglio F, Walter R, Schwartz IL. Conformational studies on neurohypophyseal hormones: The disulfide bridge of oxytocin. *Proc. Natl Acad. Sci. USA* 1968; **60**: 967–974.
68. Fric I, Kodícek M, Jost K, Bláha K. Chiroptical properties of carba-analogues of oxytocin: Conformational considerations. *Collect. Czech. Chem. Commun.* 1974; **39**: 1271–1289.
69. Bodanszky M, Stahl GL. Structure and synthesis of malformin A1. *Bioorg. Chem.* 1975; **4**: 93–105.
70. Bodanszky M, Stahl GL, Curtis RW. Synthesis and biological activity of enantio-[5-valine]malformin, a palindrome peptide. *J. Am. Chem. Soc.* 1975; **97**: 2857–2859.
71. Casey JP, Martin RB. Disulfide stereochemistry. Conformations and chiroptical properties of L-cystine derivatives. *J. Am. Chem. Soc.* 1972; **94**: 6141–6151.
72. Carmack M, Neubert LA. Circular dichroism and the absolute configuration of the chiral disulfide group. *J. Am. Chem. Soc.* 1967; **89**: 7134–7136.
73. Ludescher U, Schwyzer R. On the chirality of the cystine disulfide group: assignment of helical sense in a model compound with a dihedral angle greater than ninety degrees using NMR and CD. *Helv. Chim. Acta* 1971; **54**: 1637–1644.
74. Bodanszky M, Henes JB. Synthesis and properties of the cyclopentapeptide desthiomalformin. *Bioorg. Chem.* 1975; **4**: 212–218.
75. Linderberg J, Michl J. On the inherent optical activity of organic disulfides. *J. Am. Chem. Soc.* 1970; **92**: 2619–2625.
76. Woody RW. Application of the Bergson model to the optical properties of chiral disulfides. *Tetrahedron* 1973; **29**: 1273–1283.
77. Coleman DW, Blout ER. The optical activity of the disulfide bond in L-cystine and some derivatives of L-cystine. *J. Am. Chem. Soc.* 1968; **90**: 2405–2416.
78. Donzel B, Kamber B, Wüthrich K, Schwyzer R. A chiral cystine disulfide group without inherent optical activity in the long-wavelength region (1H- and 13C-NMR, UV, CD, and ORD. Studies with cyclo-L-cystine). *Helv. Chim. Acta* 1972; **55**: 947–961.
79. Kotelchuck D, Scheraga HA, Walter R. Conformational energy studies of oxytocin and its cyclic moiety. *Proc. Natl Acad. Sci. USA* 1972; **69**: 3629–3633.
80. Nikiforovich GV, Leonova VI, Galaktionov SG, Chipens GI. Theoretical conformational analysis of oxytocin molecule. *Int. J. Pept. Protein Res.* 1979; **13**: 363–373.
81. Hagler AT, Osguthorpe DJ, Dauber-Osguthorpe P, Hempel JC. Dynamics and conformational energetics of a peptide hormone: Vasopressin. *Science* 1985; **227**: 1309–1315.
82. Ward DJ, Chen E, Platt E, Robson B. Development and testing of protocols for computer-aided design of peptide drugs, using oxytocin. *J. Theor. Biol.* 1991; **148**: 193–227.
83. Bhaskaran R, Chuang L-C, Yu C. Conformational properties of oxytocin in dimethyl sulfoxide solution: NMR and restrained molecular dynamics studies. *Biopolymers* 1992; **32**: 1599–1608.
84. Shenderovich M, Balodis J, Mishlyakova N, Liwo A, Kasprzykowski F, Kaspryzkowska R, Tarnowska M, Ciarkowski J. In *Peptides 1992. Proceedings of the 22nd European Peptide Symposium*, Schneider CH, Eberle AN (eds). ESCOM: Leiden, 1993; 535–536.
85. Hill PS, Smith DD, Slaninova J, Hruby VJ. Bicyclization of a weak oxytocin agonist produces a highly potent oxytocin antagonist. *J. Am. Chem. Soc.* 1990; **112**: 3110–3113.
86. Smith DD, Slaninova J, Hruby VJ. Structure-activity studies of a novel bicyclic oxytocin antagonist. *J. Med. Chem.* 1992; **35**: 1558–1563.
87. Tarnowska M, Liwo A, Shenderovich M, Liepina I, Golbraikh AA, Gronzka Z, Tempczyk A. A molecular mechanics study of the effect of substitution in position 1 on the conformational space of the oxytocin/vasopressin ring. *J. Comput. Aided Mol. Des.* 1993; **7**: 699–720.
88. Cahn RS, Ingold C, Prelog SV. Specification of molecular chirality. *Angew. Chem. Int. Ed.* 1966; **5**: 385–415.
89. Koch HP. Absorption spectra and structure of organic sulfur compounds. Part II. disulfides and polysulphides. *J. Chem. Soc.* 1949; 394–401.

